Received 7 March 2007
Revised 26 February 2008
Accepted 12 March 2008

Boundary transfer operators in one-way nesting schemes for heat flow problems

Evgeny Shavelzon and Dan Givoli
Department of Aerospace Engineering, Technion, Israel Institute of Technology, Haifa, Israel

Abstract

Purpose – The interaction of a global model (GM) and a local (regional) model (LM) of heat flow is considered under the framework of so-called "one-way nesting". In this framework, the GM is constructed in a large domain with coarse discretization in space and time, while the LM is set in a small subdomain with fine discretization.

Design/methodology/approach – The GM is solved first, and its results are then used via some *boundary transfer operator* (BTO) on the GM–LM interface in order to solve the LM. Past experience in various fields of application has shown that one has to be careful in the choice of BTO to be used on the GM–LM interface, since this choice affects both the stability and accuracy of the computational scheme. Here the problem is first theoretically analyzed for the linear heat equation, and stable BTOs are identified. Then numerical experiments are performed with one-way nesting in a two-dimensional channel for heat flow with and without radiation emission and linear reaction, using four different BTOs.

Findings – Among other conclusions, it is shown that the "negative Robin" BTO is unstable, whereas the Dirichlet, Neumann and "positive Robin" BTO are all stable. It is also shown that in terms of accuracy, the Neumann and "positive Robin" BTOs should be preferred over the Dirichlet BTO.

Originality/value – This study may be the first step in analyzing BTO accuracy and stability for more general atmospheric systems.

Keywords Heat, Flow, Modeling

Paper type Research paper

1. Introduction

The multiscale procedure called "nesting" is often used in various fields of application involving unbounded or very large domains, like weather prediction, oceanography and solid earth geophysics. See, e.g., the early review paper (Sundström and Elvius, 1979) and the recent book (Kalnay, 2003). See also the more recent papers (Warner *et al.*, 1997; Staniforth, 1997; Laprise, 2003) on nesting in the context of atmospheric models. In this procedure, two or more numerical models of different spatial and temporal scales interact with each other. In the simplest and most common case only two models are considered: a Global Model (GM) and a Local Model (LM) which is also called regional or limited-area model. See the setup illustrated in Figure 1.

Using the nesting scenario considered in Numerical Weather Prediction (NWP) (Kalnay, 2003; Haltiner, 1980) as a prototype, the GM is related to the solution of the atmospheric equations over the entire spherical surface of the globe Ω_G, while in the LM, the solution is sought in a relatively small region Ω_L bounded by an artificial boundary Γ. The GM captures the large-scale atmospheric phenomena and is based on a coarse grid (about 100 km resolution) and large time steps, whereas the LM captures

This research was supported by the Israel Science Foundation (ISF) grant number 797/06, by the Fund for the Promotion of Research at the Technion and by the fund provided through the Lawrence and Marie Feldman Chair in Engineering.

International Journal of Numerical Methods for Heat & Fluid Flow
Vol. 19 Nos. 3/4, 2009
pp. 352-373

0961-5539
DOI 10.1108/09615530910938326

the mesoscale phenomena and is based on a finer grid (typically 10-20 km resolution) and much smaller time steps. Typically, the GM and LM are solved by using entirely different numerical methods (and different computer codes). For example, the US Navy code NOGAPS (Rosmond, 1992) is a GM-solver based on a global Galerkin method in spherical coordinates, while the Navy's code COAMPS (Hodur, 1997) is a LM-solver based on finite differences in Cartesian coordinates.

Nesting may be *one-way* or *two-way*. One-way nesting is simpler and is more common in practice; see, e.g., recent applications in Ju and Wang (2006), Antic *et al.* (2006), Jimenez, *et al.* (2007) and Xin *et al.* (2004). In one-way nesting, the global problem is solved first (via the GM) and then the regional problem is solved (via the LM) *while taking into account the relevant GM results*. In two-way nesting the GM and LM solutions are fully coupled and affect each other; see, e.g. (Phillips and Shukla, 1973; Sundström and Elvius, 1979) for a basic discussion on this subject in the context of NWP, and (Barth *et al.*, 2005) for a recent two-way nested model. The US Navy uses mainly the Davies scheme (Davies, 1976) for lateral one-way nesting. We shall consider here only one-way nesting and assume that no additional solution of the global problem beyond the single given GM solution is available or desired.

One major way to pass the information from the GM to the LM in one-way nesting is through a *boundary condition* on the interface Γ. Although the GM solution is available in the entire domain Ω_L, it is reasonable to leave the task of evolving the solution in the interior of Ω_L to the LM alone, since it uses much finer discretization than that of the GM and therefore is potentially much more accurate. Moreover, the *initial data* defined for the LM are also typically much finer in resolution than the initial data provided for the GM. Thus, it is reasonable to construct the one-way nesting scheme such that the information is passed from the GM to the LM only through the boundary Γ. The boundary condition used on Γ in the LM is needed for the closure of the mathematical problem in Ω_L, namely to make the problem in Ω_L well-posed.

Denoting the GM solution $\mathbf{u}_G$ and the LM solution $\mathbf{u}_L$, we first find $\mathbf{u}_G$ by solving the global problem. Then we use a boundary condition of the general form

$$\mathbf{B}\mathbf{u}_L = \mathbf{B}\mathbf{u}_G \quad \text{on } \Gamma \tag{1}$$

for the closure of the LM. Here $\mathbf{B}$ is a linear differential operator defined on the boundary, which may be called a *boundary transfer operator* (BTO). Two simple examples for BTOs are theidentity, which turns Equation (1) into the Dirichlet boundary condition

$$\mathbf{u}_L = \mathbf{u}_G \quad \text{on } \Gamma, \tag{2}$$

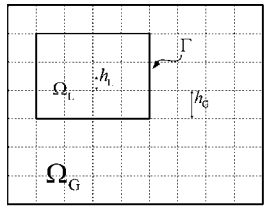

Notes: Shown are the global domain Ω_G, the local (regional) domain Ω_L, the global-regional interface Γ (which is the boundary of Ω_L) and the meshes used for the two models

Figure 1.
Setup for a nesting procedure

and the normal derivative, in which case (1) becomes the Neumann boundary condition

$$\frac{\partial \mathbf{u}_L}{\partial_n} = \frac{\partial \mathbf{u}_G}{\partial_n} \quad \text{on } \Gamma. \tag{3}$$

It should be remarked that on the discrete level, the BTOs appearing on the left and right sides of Equation (1) are not identical, due to the different resolutions of the LM and GM. A more careful notation would be

$$\mathbf{B}_L \mathbf{u}_L = \mathbf{B}_{GL} \mathbf{u}_G \quad \text{on } \Gamma, \tag{4}$$

where the operator $\mathbf{B}_L$ is directly defined on the LM-scale, while the operator $\mathbf{B}_{GL}$ involves both the GM and LM-scale. There are actually two ways in which $\mathbf{B}_{GL}$ may be defined; either by first taking discrete differentials on the GM-scale and then interpolating the data from the GM-scale to the LM-scale, or by first interpolating and then taking the discrete differentials. We shall remark on this issue later in the sequel.

It should also be noted that BTOs not only appear in nesting schemes but also constitute a major mechanism of transferring data in Domain Decomposition methods; see, e.g., the related papers in (Raspo *et al.*, 1996; Gerardo-Giroda *et al.,* 2004; Portero and Jorge, 2005; Barlett *et al.,* 2006; Heinkenschloss and Herty, 2007; and Hauret and Le Tallec *et al.*, 2007). Nonlocal operators are also used as BTOs; the most prominent example is the Dirichlet-to-Neumann map (Yang and Yu, 2006; Magoules *et al.*, 2006a, b; Hughes, 1995; Givoli, 1999) which is known to be optimal in a certain sense. However, in this paper we shall restrict ourselves to the more common use of local (differential) BTOs which are generally believed to be more economical computationally.

There are two aspects in which the soundness of using a specific BTO in Equation (1) should be examined: *stability* and *accuracy*. Certain BTOs may lead to numerical instabilities by giving rise to spurious modes. It is therefore important, for a given type of problem, to characterize those BTOs which are stable and those which are not. For the linear wave equation, such analysis was carried out in Mar-Or and Givoli (2006), here we shall perform similar analysis for the linear *heat equation*. As to accuracy, the potential for poor performance of a given BTO exists, since there is a clear incompatibility between the GM and LM, on both the physical level (two different scales of physical phenomena) and the numerical level (non-matching discretizations in space and time), that may cause significant errors to be generated on the interface Γ. By using numerical experiments, the accuracy of several BTOs was investigated for the wave equation in Mar-Or and Givoli (2006, 2009). Here we shall conduct numerical experiments to examine the accuracy of four basic BTOs for the two dimensional (nonlinear) heat equation in a channel, with or without radiation emission and linear reaction.

For completeness, we mention an alternative approach, namely that of using variable resolution or stretched grids, to allow local increase of resolution in global models. See, e.g. (Fox-Rabinovitz *et al.*, 2005; SGMIP). A different approach to lateral boundary-condition nesting is called the "(spectral) nudging of the large scales;" see, e.g. (Miguez-Macho *et al.*, 2004; von Storch *et al.*, 2000). Finally we mention a GM–LM interaction scheme which is not used, to the best of our knowledge, by the NWP community. This is Fish's *s*-version of the finite element method (Fish, 1992), where the local fine mesh is superposed as a patch upon the global coarse mesh, and the global and local problems are solved *simultaneously*. Application of such a scheme in NWP may prove to be effective although it may entail serious technical difficulties. However,

it is not so practical if one is interested in solving the GM problem only once and then many different regional problems.

Following is the outline of the rest of the paper. In Section 2, we provide the statement of the one-way nesting problem for the heat equation in a two-dimensional channel. In Section 3, we theoretically analyze the linear heat equation and identify the stable BTOs out of a general class. In Section 4, we discuss the finite element (FE) formulation and some computational aspects of the scheme. We then present the results of several numerical experiments in Section 5, and we draw conclusions regarding the choice of appropriate BTOs. We close with some concluding remarks in Section 6.

2. Statement of the one-way nesting problem

We consider a one-way nesting configuration for the temperature field in a two-dimensional channel, as illustrated in Figure 2. The channel is of width b and is bounded on the north and south sides by the "walls" Γ_N and Γ_S on which we impose homogeneous Dirichlet boundary conditions (zero temperature). Cartesian coordinates $\mathbf{x} = (x, y)$ are used, such that Γ_S and Γ_N lie along $y = 0$ and $y = b$, respectively. On the west side the domain is bounded by Γ_W on which we prescribe given Dirichlet values. The global domain Ω_G constitutes the entire channel. On the east side Ω_G is bounded by Γ_∞, which may be placed at infinity or at a finite location, and on which a far-field temperature value is prescribed. In our numerical experiments, we consider a finite Ω_G, since the unboundedness of the global domain is not a central issue here. The local domain Ω_L is bounded on the west, south and north sides by Γ_W, Γ_S and Γ_N, respectively (where using Γ_S and Γ_N for both the GM and LM involves a slight abuse of notation). On the east side, Ω_L is bounded by the GM–LM interface $\Gamma_E \equiv \Gamma$, which is located at $x = a$.

The GM problem for the global temperature field $u_G(\mathbf{x}, t)$ is given by

$$\rho c \frac{\partial u_G}{t} + \gamma u_G + r u_G^4 - \nabla \cdot \kappa \nabla u_G = f^G(\mathbf{x}, t) \quad \text{in } \Omega_G, \tag{5}$$

$$u_G = g^G(y, t) \quad \text{on } \Gamma_W, \tag{6}$$

$$u_G = 0 \quad \text{on } \Gamma_S \ \& \ \Gamma_N, \tag{7}$$

$$u_G = u_\infty \quad \text{on } \Gamma_\infty, \tag{8}$$

$$u_G(\mathbf{x}, 0) = u_0^G(\mathbf{x}) \quad \text{in } \Omega_G. \tag{9}$$

Here ρ is the mass density, c is the heat capacity, γ is the linear reaction coefficient, r is the radiation emission coefficient and κ is the heat conductivity. From physical reasons we assume that $\rho c > 0, \kappa > 0$ and $r \geq 0$, while no sign restriction is put on γ. The functions u_∞, f^G, g^G and u_0^G represent given GM-scale

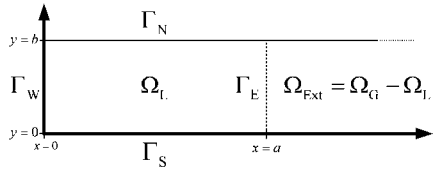

Figure 2.
Setup for the two-dimensional channel problem

far-field temperature, distributed wave sources, Dirichlet boundary data and initial data, respectively.

The LM problem for the local temperature field $u_L(\mathbf{x}, t)$ is given by

$$\rho c \frac{\partial u_L}{t} + \gamma u_L + r u_L^4 - \nabla \cdot \kappa \nabla u_L = f^L(\mathbf{x}, t) \quad \text{in } \Omega_L, \tag{10}$$

$$u_L = g^L(y, t) \quad \text{on } \Gamma_W, \tag{11}$$

$$u_L = 0 \quad \text{on } \Gamma_S \ \& \ \Gamma_N, \tag{12}$$

$$\mathcal{B} u_L = \mathcal{B} u_G \quad \text{on } \Gamma_E, \tag{13}$$

$$u_L(\mathbf{x}, 0) = u_0^L(\mathbf{x}) \quad \text{in } \Omega_L. \tag{14}$$

Here the functions f^L, g^L and u_0^L are the LM-scale analogs of the GM functions f^G, g^G and u_0^G, respectively. In Equation (13) the global solution is transferred to the LM problem through the BTO $\mathcal{B}$ acting on the interface Γ_E.

Our goal is to examine the stability and accuracy of the LM solution u_L for different BTOs $\mathcal{B}$.

3. Stability analysis

A partial differential equation in the domain Ω_L may be associated with normal modes or eigenfunctions. Some of these modes may not be present in the original problem defined in the domain Ω_G. When one considers the LM problem in Ω_L, these modes should not be excited in theory, but even the smallest numerical error (e.g. round off) *would* excite them and hamper the accuracy of the numerical results. Analysis of these modes can be done on the continuous level (rather than on the discrete level) by considering a small perturbation of the equations constituting the problem.

We illustrate this first with a simple one-dimensional example. We consider the following heat-flow toy problem for the temperature field $u(x, t)$:

$$u'' = \ddot{u}, \qquad 0 < x < 1, \tag{15}$$

$$u'(0, t) = 0, \tag{16}$$

$$u'(1, t) - u(1, t) = 0, \tag{17}$$

$$u(x, 0) = 0. \tag{18}$$

Here a prime and a dot denote differentiation with respect to x and t, respectively. The trivial solution $u \equiv 0$ is the only solution for this problem.

We wish to consider "modes" that satisfy Equations (15)-(17), of the exponentially-growing form

$$u(x, t) = A \cosh(\mu x) \exp(\mu^2 t), \tag{19}$$

where A and $\mu \geq 0$ are constants. It is easy to verify that u given by Equation (19) satisfies the heat Equation (15) and the left boundary condition Equation (16) identically. If we insist that it also satisfy the right boundary condition Equation (17)

we get the equation for μ,

$$\mu = \coth(\mu). \tag{20}$$

This equation has a single root, which is $\mu = \mu_0 \simeq 1.2$. Thus, Equation (19) with $\mu = \mu_0$ indeed satisfies Equations (15)-(17). Imposing in addition the initial condition Equation (18) on u in Equation (19) leads to the unique solution $u \equiv 0$.

Now, suppose we perturb the initial condition Equation (18) slightly. In particular, we replace Equation (18) by

$$u(x, 0) = \epsilon \cosh(\mu_0 x), \tag{21}$$

where ϵ is a small number. Then from Equation (19) it is clear that the solution to the problem becomes

$$u(x, t) = \epsilon \cosh(\mu_0 x) \exp(\mu_0^2 t), \tag{22}$$

which grows exponentially in time. Thus, an $O(\epsilon)$ perturbation in the initial condition leads to an *unbounded* solution! Clearly, this is an unstable situation and constitutes an example of a spurious mode which awakens to the slightest perturbation. A similar example may be constructed where the perturbation is not in the initial conditions but in the boundary conditions or in the heat equation itself (i.e. a perturbation of the equation by a small inhomogeneous term).

It can be shown that the cause for the instability just described is the boundary operator used in Equation (17). If this operator was replaced by, say, the identity (namely Equation (17) was replaced by the Dirichlet condition $u = 0$) no spurious mode would have been present. This has an immediate relevance to the choice of the BTO for the GM–LM interaction problem described in Section 2. In order to guarantee stability of the scheme, we need to employ a BTO which does not admit spurious modes.

To characterize the boundary operators which do not give rise to such modes, we consider a finite spatial domain Ω (in any dimension) with boundary Γ. In Ω we consider the homogeneous linear heat equation

$$\rho c \frac{\partial u}{\partial t} + \gamma u - \nabla \cdot \kappa \nabla u = 0 \quad \text{in } \Omega, \tag{23}$$

where $\rho c > 0, \kappa > 0$ and γ may be functions of location. A discussion related to the sign of γ will follow shortly.

We append the heat Equation (23) with a boundary condition of the form

$$\mathcal{B}u \equiv \delta \frac{\partial u}{\partial n} + \alpha u + \beta \frac{\partial u}{\partial t} = 0 \quad \text{on } \Gamma, \tag{24}$$

where $\partial u/\partial n$ is the outward normal derivative of u on Γ, and δ, α and β are real functions of location on Γ. We assume that at points where $\delta = 0$ on Γ, α and β do not vanish simultaneously, otherwise no boundary condition would be given at such points. The boundary condition Equation (24) is quite general. Mixed condition types on Γ (e.g. Dirichlet condition on one part of Γ and Neumann condition on the other part of Γ) are represented in Equation (24) by using appropriate coefficient functions $\delta(\mathbf{x}), \alpha(\mathbf{x})$ and $\beta(\mathbf{x})$. The goal is to find restrictions on δ, α and β such that no

spurious modes be present. Such restrictions would guarantee that the operator $\mathcal{B}$ in Equation (24) is stable when used as a BTO in a GM–LM one-way nesting scheme.

We do not restrict the sign of the reaction coefficient γ in Equation (23), but we note that for a sufficiently large negative γ, Equation (23) may admit exponentially growing solutions. We assume that this is not the case, namely that $\gamma(\mathbf{x})$ is such that the exact solution is decaying in time. A sufficient condition for this can be stated by defining the associated "Rayleigh quotient"

$$R[\tilde{\boldsymbol{u}}] = \frac{\int_\Omega \kappa|\nabla\tilde{\boldsymbol{u}}|^2 d\Omega + \int_{\Omega_\gamma^+} \gamma|\tilde{\boldsymbol{u}}|^2 d\Omega}{\int_{\Omega_\gamma^-} |\gamma||\tilde{\boldsymbol{u}}|^2 d\Omega}, \quad \tilde{\boldsymbol{u}} \in \mathcal{S}. \tag{25}$$

Here Ω_γ^+ is the part of Ω in which $\gamma \geq 0$, Ω_γ^- is the part of Ω in which $\gamma < 0$, and $\mathcal{S}$ is the function space defined by

$$\mathcal{S} = \{\tilde{\boldsymbol{u}} | \tilde{\boldsymbol{u}} \in H^1(\Omega) \quad \& \quad \tilde{\boldsymbol{u}} = 0 \quad \text{on } \Gamma_0\}, \tag{26}$$

where H^1 is the Sobolev space of functions with square-integrable 0th and 1st derivatives, and Γ_0 is the part of Γ on which $\delta = 0$ (namely the part of Γ where an essential boundary condition is imposed). It can be shown that if γ is such that

$$R[\tilde{\boldsymbol{u}}] \geq 1 \quad \text{for all} \quad \tilde{\boldsymbol{u}} \in \mathcal{S}, \tag{27}$$

then any solution satisfying Equations (23) and (24) decays in time. This is implied by the fact that the condition Equation (27) guarantees that all the eigenvalues of the associated eigenvalue problem have a non-negative real part; see, e.g. (Courant and Hilbert, 1989). We shall assume that Equation (27) indeed holds.

The analysis that follows is somewhat reminiscent of the "principle of exchange of stability"; see, e.g. (Drazin and Reid, 2004). We shall restrict the spurious-mode analysis to modes of complex exponential form in time, i.e., we shall consider solutions of the form

$$u(\mathbf{x}, t) = \hat{\boldsymbol{u}}(\mathbf{x}; \mu)e^{\mu t}, \quad \mu = \sigma + i\omega. \tag{28}$$

Here σ and ω are real numbers, where $\sigma \geq 0$, namely we consider exponentially growing modes, pure oscillatory modes and their combination, as well as the stationary mode ($\mu = 0$). Substituting Equation (28) into Equation (23) and Equation (24) yields

$$(\gamma + \rho c\mu)\hat{\boldsymbol{u}} - \nabla \cdot \kappa\nabla\hat{\boldsymbol{u}} = 0 \quad \text{in } \Omega, \tag{29}$$

$$\delta\partial\hat{\boldsymbol{u}}/\partial n + (\alpha + \mu\beta)\hat{\boldsymbol{u}} = 0 \quad \text{on } \Gamma. \tag{30}$$

Now we multiply Equation (29) by $\hat{\boldsymbol{u}}^*$, the complex conjugate of $\hat{\boldsymbol{u}}$, and integrate over Ω to obtain

$$\int_\Omega \hat{\boldsymbol{u}}^*[(\gamma + \rho c\mu)\hat{\boldsymbol{u}} - \nabla \cdot \kappa\nabla\hat{\boldsymbol{u}}]d\Omega = 0. \tag{31}$$

We apply the divergence theorem to the second term on the left of Equation (31) and

use Equation (30) to get

$$\int_{\Omega}[(\gamma+\rho c\mu)|\hat{\boldsymbol{u}}|^2+\kappa|\nabla\hat{\boldsymbol{u}}|^2]d\Omega+\int_{\tilde{\Gamma}}\frac{\kappa(\alpha+\mu\beta)}{\delta}|\hat{\boldsymbol{u}}|^2d\Gamma=0. \tag{32}$$

Here $\tilde{\Gamma}$ is defined as the part of Γ on which $\delta \neq 0$. Note that from Equation (30), $\hat{\boldsymbol{u}}=0$ at points on Γ where $\delta=0$, hence the boundary term in Equation (32) vanishes at these points.

Now we write Equation (32) as two equations, for the real and imaginary parts of the expressions:

$$\int_{\Omega}[(\rho c\sigma+\gamma)|\hat{\boldsymbol{u}}|^2+\kappa|\nabla\hat{\boldsymbol{u}}|^2]d\Omega+\int_{\tilde{\Gamma}}\frac{\kappa(\alpha+\sigma\beta)}{\delta}|\hat{\boldsymbol{u}}|^2d\Gamma=0, \tag{33}$$

$$\omega\left[\int_{\Omega}\rho c|\hat{\boldsymbol{u}}|^2d\Omega+\int_{\tilde{\Gamma}}\frac{\kappa\beta}{\delta}|\hat{\boldsymbol{u}}|^2d\Gamma\right]=0. \tag{34}$$

A sufficient condition for $\hat{\boldsymbol{u}}$ to be identically zero (and thus to be mode-less) is that the left side of at least one of the Equations (33) and (34) be strictly positive unless $\hat{\boldsymbol{u}}\equiv 0$. Careful investigation of Equations (33) and (34) in various cases, while making use of Equation (27), leads to the following conclusions:

(1) In the special case where $\delta\equiv 0$ on Γ, i.e. *Dirichlet boundary condition is applied all over the boundary*, it is easy to see from Equation (34) that no oscillatory modes ($\omega\neq 0$) are present. Owing to Equation (27), it is clear that pure exponential modes ($\omega=0,\sigma>0$) are also suppressed. Thus, the use of the identity operator as a BTO is safe as far as stability is concerned. The following cases assume that $\tilde{\Gamma}$ is not empty.

(2) *To prevent pure exponentially-growing modes* ($\omega=0,\sigma>0$) it is sufficient to have

$$\alpha(\mathbf{x})/\delta(\mathbf{x})\geq 0,\ \ \beta(\mathbf{x})/\delta(\mathbf{x})\geq 0 \quad \text{on } \tilde{\Gamma}. \tag{35}$$

(3) *To prevent pure oscillatory modes* ($\sigma=0,\omega\neq 0$) it is sufficient to have either

$$\alpha(\mathbf{x})/\delta(\mathbf{x})\geq 0 \quad \text{on } \tilde{\Gamma}. \tag{36}$$

or

$$\beta(\mathbf{x})/\delta(\mathbf{x})\geq 0 \quad \text{on } \tilde{\Gamma} \tag{37}$$

(4) *To prevent combined oscillatory and exponentially-growing modes* ($\sigma>0,\omega\neq 0$) it is sufficient to have

$$\beta(\mathbf{x})/\delta(\mathbf{x})\geq 0 \quad \text{on } \tilde{\Gamma}. \tag{38}$$

(5) *To prevent the stationary mode* ($\sigma = 0, \omega = 0$) it is sufficient to have

$$\alpha(\mathbf{x})/\delta(\mathbf{x}) \geq 0 \quad \text{on } \tilde{\Gamma}. \tag{39}$$

(6) *To prevent all modes above* it is sufficient to have

$$\alpha(\mathbf{x})/\delta(\mathbf{x}) \geq 0, \quad \beta(\mathbf{x})/\delta(\mathbf{x}) \geq 0 \quad \text{on } \tilde{\Gamma}. \tag{40}$$

The conditions above become very simple in some specific cases. For example, the Dirichlet condition $u = 0$, the Neumann condition $\partial u/\partial n = 0$ and the "positive Robin" condition $\partial u/\partial n + \alpha u = 0$ for $\alpha > 0$, all do not admit spurious modes. On the other hand, the "negative Robin" condition $\partial u/\partial n - \alpha u = 0$ for $\alpha > 0$, is not safe since it is not guaranteed to reject spurious modes. Indeed, we shall see via numerical experiments that when the "negative Robin" operator is used as a BTO, it generates instability, while other basic BTOs are stable.

It should be remarked that the conditions provided by the analysis above are only *sufficient*. Thus, it may be the case that a certain BTO which does not satisfy some of these conditions would turn out to be nevertheless stable.

4. Finite element formulation and computational aspects

We will briefly outline the FE formulation used for solving the LM. The GM is solved (first) in the same way, although the formulation is slightly simpler for the GM because no BTO is involved.

We consider the solution of the LM problem Equations (10)-(14). We omit the index L from the LM variables for clarity. The statement of the problem is

$$\rho c \frac{\partial u}{\partial t} + \gamma u + r u^4 - \nabla \cdot \kappa \nabla u = f(\mathbf{x}, t) \quad \text{in } \Omega_L \tag{41}$$

$$u = g \quad \text{on } \Gamma_W, \tag{42}$$

$$u = 0 \quad \text{on } \Gamma_S \,\&\, \Gamma_N, \tag{43}$$

$$\delta \frac{\partial u}{\partial n} + \alpha u = \delta q_G + \alpha u_G \quad \text{on } \Gamma_E, \tag{44}$$

$$u(\mathbf{x}, 0) = u_0(\mathbf{x}) \quad \text{in } \Omega_L. \tag{45}$$

In Equation (44), we consider the BTO

$$B \equiv \delta \frac{\partial}{\partial n} + \alpha \tag{46}$$

and ignore the more exotic time-derivative term in Equation (24). The q_G in Equation (44) is a given function defined roughly as

$$q_G = \frac{\partial u_G}{\partial n} \quad \text{on } \Gamma_E; \tag{47}$$

however one should keep in mind that $\partial u_G/\partial n$ is (for C^0 FEs) a discontinuous function which is given on the GM-scale, while q_G must be single valued and should be provided on the LM-scale. We will touch upon this point later.

The weak form of the problem Equations (41)-(45) is as follows:
Find $u \in \mathcal{S}$ such that for all $w \in \mathcal{S}_0$

$$(w, \rho c\dot{u}) + a(w,u) = L(w), \tag{48}$$

$$(w, u(\mathbf{x},0)) = (w, u_0(\mathbf{x})), \tag{49}$$

where

$$\mathcal{S} = \{\ u \mid u \in H^1(\Omega), \quad u = g \quad \text{on } \Gamma_W, \quad u = 0 \quad \text{on } \Gamma_S \cup \Gamma_N \cup \Gamma_0\ \}, \tag{50}$$

$$\mathcal{S}_0 = \{\ w \mid w \in H^1(\Omega), \quad w = 0 \quad \text{on } \Gamma_W \cup \Gamma_S \cup \Gamma_N \cup \Gamma_0\ \}, \tag{51}$$

$$(w,f) = \int_\Omega wf\, d\Omega, \tag{52}$$

$$a(w,u) = \int_\Omega \nabla w \cdot \kappa \nabla u d\Omega + \int_\Omega w\gamma u\, d\Omega + \int_\Omega wru^4\, d\Omega + \int_{\tilde{\Gamma}} w\frac{\kappa\alpha}{\delta} u\, d\Gamma, \tag{53}$$

$$L(w) = \int_\Omega wf d\Omega + \int_{\tilde{\Gamma}} w\kappa\left(q_G + \frac{\alpha u_G}{\delta}\right) d\Gamma. \tag{54}$$

We recall that Γ_0 is defined as the part of the GM–LM interface Γ_E along which $\delta = 0$, namely where an essential boundary condition is imposed, whereas $\tilde{\Gamma}$ is the other part of Γ_E, where $\delta \neq 0$. We note that the form $a(\cdot,\cdot)$ is nonlinear in its second slot, unless $r = 0$ (no radiation) in which case $a(\cdot,\cdot)$ is a symmetric bilinear form.

Discretization of the weak form of the problem by FEs leads to the following semi-discrete problem in time:

$$\mathbf{M}\dot{\mathbf{d}}(t) + \mathbf{G}(\mathbf{d}(t)) = \mathbf{F}(t). \tag{55}$$

$$\mathbf{d}(0) = \mathbf{d}_0, \tag{56}$$

where $\mathbf{d}$ is the temperature vector whose entries are the nodal temperatures, $\mathbf{d}_0$ is the vector of initial temperatures, $\mathbf{M}$ is the heat capacity matrix, $\mathbf{G}(\mathbf{d})$ is the nonlinear heat-flux vector, and $\mathbf{F}$ is the thermal load vector. On the global level, the expressions for these arrays are given by

$$M_{IJ} = (N_I, \rho c N_J), \tag{57}$$

$$G_I(\mathbf{d}) = a\left(N_I, \sum_{J=1}^{N_{np}} N_J d_J\right), \tag{58}$$

$$F_I = L(N_I). \tag{59}$$

Here N_I is the global FE shape-function associated with global node I, and N_{np} is the total number of nodal points. We note that from Equations (58) and (53), the heat flux vector **G** represents the effects of conductivity, linear reaction, radiation emission, and also the "pulling" part of the BTO. The "pushing" part of the BTO is taken care of by the load vector **F**, as evident from Equations (59) and (54). Of course, in practice all the FE arrays are calculated on the element level, using expressions analog to Equations (57)-(59). See (Zienkiewicz and Taylor, 2000) for further details.

We solve the semi-discrete problem Equations (55) and (56) by using the standard implicit 2nd-order Crank-Nicolson time-stepping scheme (Hughes, 1987). If the problem is nonlinear ($r \neq 0$) then we perform Newton iterations within each time-step, using the exact tangent stiffness matrix (Zienkiewicz and Taylor, 2000). The computational effort involved in the nonlinear case is quite large; however, our goal is to compare the accuracy and stability of various local BTOs, and since the computing times associated with each of these BTOs is about the same, relative efficiency is not an issue here.

A final issue that must be explained is the calculation *on the LM-scale* of the functions u_G and q_G which are originally generated *on the GM-scale*. These functions appear in Equations (44) and (54), and we recall that q_G is a regularized measure of the normal derivative of u_G on Γ_E, as in Equation (47). The difference in scale is both in space (meshes of different densities) and in time (different time-step sizes). The coarse-to-fine passage of information is performed in two steps: first we calculate a regularized quantity on the GM-scale, and second we pass the information to the LM-scale via linear interpolation is space and in time. Regularization of the function u_G itself is not generally needed. On the other hand, the normal derivative q_G does require some post-process smoothing, because it is discontinuous across element boundaries, and hence suffers a jump on Γ_E. Various smoothing schemes which are in fact "flux-recovery" schemes (Zienkiewicz and Taylor, 2000), may be applied. In our numerical experiments, we chose to employ a simple 2nd-order central finite difference 3-node stencil to calculate the normal derivative of q_G at the Γ_E nodes. After the GM-nodal values are determined, linear interpolation is assumed for points between them.

Our numerical experiments and other considerations Mar-Or and Givoli (2006, 2009) show that for non-smooth data it is *much preferable to first regularize the data on the coarse scale and then pass it to the fine scale* than first to pass the information and only then to regularize it.

5. Numerical experiments and discussion

We consider a two-dimensional channel, with the setup shown in Figure 2. The GM and LM equations are given by Equations (5)-(9) and Equations (10)-(14), respectively, where we assume no distributed sources ($f^G = f^L = 0$). We set $\rho c = 1$ and $\kappa = 1$. The width of the channel is $b = 5$. The global domain Ω_G is the long rectangle $(0, a_\infty) \times (0, b)$, where $a_\infty = 20$. The GM–LM interface Γ_E is set by default to $a = 5$, namely the LM domain is a quarter of the GM domain, although we shall also consider the case $a = 2$, where the LM is much smaller. To solve both the GM and LM problems we use bilinear quadrilateral FEs. We fix the density of the LM mesh (with a mesh parameter of $h_L = 0.125$) and the LM time-step size (with $\Delta t_L = 3.25 \cdot 10^{-4}$), but we vary the density of the GM mesh and time-step size in order to check the effect of different discretization ratios on the errors generated. We define the *GM–LM mesh ratio* as $\mathrm{MR} = h_G/h_L$. We try three possible mesh ratios, i.e., MR = 1:1, 2:1 and 4:1. The case MR = 1:1 is, of course, totally artificial and is meant merely for the sake of comparison. The *GM–LM time-step ratio* $\mathrm{TR} = \Delta t_G/\Delta t_L$ is chosen in each case so

that $\mathrm{TR} \simeq (\mathrm{MR})^2$, following the standard FE error estimate for linear heat-flow problems (Hughes, 1987).

In the linear cases, namely when $r = 0$ (no radiation), we synthesize an exact analytic solution in the form of a single "mode" with oscillatory behavior in space and exponential decay in time, namely

$$u(x,y,t) = \exp\left[-\left(\kappa\pi^2\left(\frac{1}{a_\infty^2}+\frac{1}{b^2}\right)+\gamma\right)\frac{t}{\rho c}\right]\sin\frac{\pi x}{a_\infty}\sin\frac{\pi y}{b}. \tag{60}$$

It is easy to verify that this solution indeed satisfies the linear heat equation and the Dirichlet condition Eqaution (7). We choose the boundary-condition functions g^G, u_∞ and g^L in Equations (6), (8) and (11) to vanish, so that u also satisfies these boundary conditions. We find the appropriate initial-value functions u_0^G and u_0^L in Equations (9) and (14) by substituting Equation (60) in these initial conditions, so that they are satisfied by u as well.

We will compare the results obtained with four different basic BTOs in Equation (13), which are special cases of Equation (44):

$$\text{Dirichlet:} \quad u_L = u_G \qquad \text{on } \Gamma_E; \tag{61}$$

$$\text{Neumann:} \quad \kappa\frac{\partial_{u_L}}{\partial n} = \kappa\frac{\partial_{u_G}}{\partial n} \quad \text{on } \Gamma_E; \tag{62}$$

$$\text{"Positive Robin"} \quad \kappa\frac{\partial_{u_L}}{\partial n} + u_L = \kappa\frac{\partial_{u_G}}{\partial n} + u_G \quad \text{on } \Gamma_E; \tag{63}$$

$$\text{"Negative Robin"} \quad \kappa\frac{\partial_{u_L}}{\partial n} - u_L = \kappa\frac{\partial_{u_G}}{\partial n} - u_G \quad \text{on } \Gamma_E. \tag{64}$$

To evaluate the LM error in each case, we consider the time-dependent relative error measure

$$E(t) = \frac{\|u_L - u_{ref}\|_{\Omega_L}}{\|u_{ref}\|_{\Omega_L}}, \tag{65}$$

where the spatial norm $\|\cdot\|_{\Omega_L}$ is the L_2 norm in Ω_L, u_L is the computed LM solution, and u_{ref} is a reference solution. For linear problems ($r = 0$), we take the reference solution to be the analytic solution Equation (60), $u_{ref} \equiv u$. For problems with heat radiation ($r \neq 0$), where an analytic solution is not available, we generate a reference solution u_{ref} by solving the problem in the GM domain Ω_G but with the fine LM discretization (the MR = 1:1 solution).

We start with the case where there is no reaction ($\gamma = 0$) and no radiation ($r = 0$). Figure 3 shows the errors $E(t)$ as defined by Equation (65), that are generated with the four BTOs and the three GM–LM mesh ratios. The following conclusions are drawn from these graphs:

- The "negative Robin" BTO is unstable, and generates an error which grows exponentially fast. All the other three BTOs are stable. This agrees with the theoretical analysis of Section 3, and will be observed in all the subsequent results as well.

- The error (in the case of the stable BTOs) grows linearly in time. This has nothing to do with the BTO, and is an unavoidable feature of the standard time-stepping scheme; see, e.g. (Hughes, 1987). Refining the discretization causes the linear growth in time to be slower.
- In the MR = 1:1 case, the Dirichlet BTO is clearly the most accurate, with an error that grows from about 0.1 per cent at $t = 1$ to below 0.2 per cent at $t = 4$. The "positive Robin" and Neumann BTOs yield errors of about 0.5 per cent and 0.6 per cent, respectively. This might lead us to the (wrong) conclusion that the

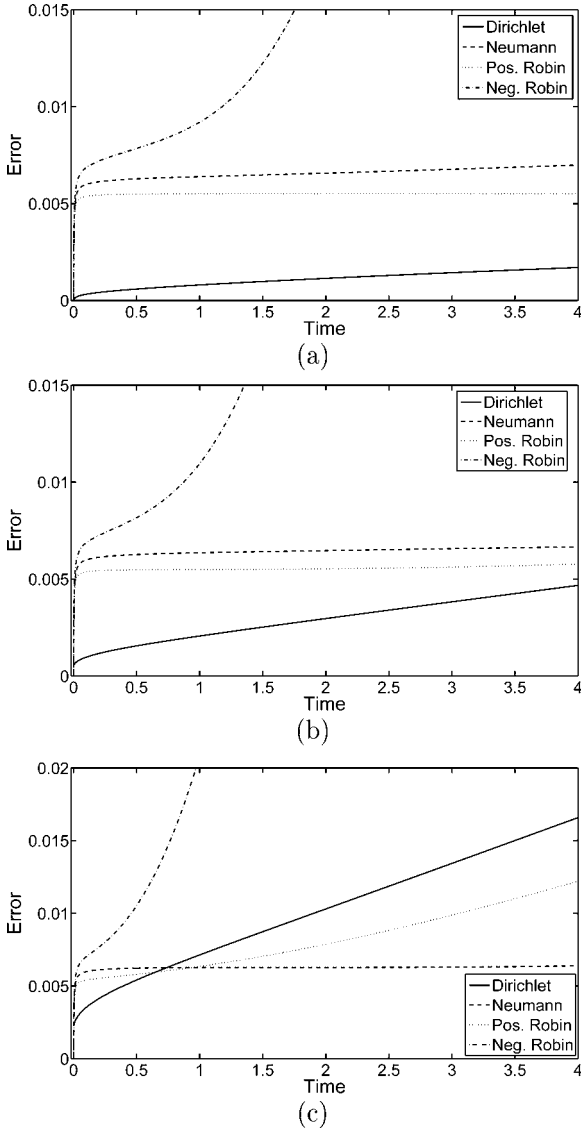

Figure 3.
Error $E(t)$ for $\gamma = 0$, $r = 0$, $a = 5$, with (a) MR $= h_G/h_L = 1$, (b) MR $= 2$, (c) MR $= 4$

Dirichlet BTO should be preferred over the other BTOs. However, see the next point.

- In the MR = 4:1 case, which is more realistic, the picture for times not very short is quite the opposite. The Dirichlet BTO is the *least accurate* and grows in time with the largest slope; it grows from about 0.75 per cent at $t = 1$ to 1.65 per cent at $t = 4$. The "positive Robin" BTO is more accurate, while the Neumann BTO yields an almost constant error level of about 0.6 per cent.

The observation that in the MR = 1:1 case the Dirichlet BTO is the most accurate while in the MR = 4:1 case it is the least accurate can be explained as follows. In the FE variational formulation, the Dirichlet boundary condition is enforced *strongly* whereas the Neumann and Robin boundary conditions are enforced *weakly*. As long as the input data are themselves sufficiently accurate, namely are consistent with the fine-scale resolution of the LM as in the MR = 1:1 case, the strong enforcement of the data is beneficial. However, when the input data themselves contain an error which is significantly larger than the LM-scale errors, as in the MR = 2:1 and MR = 4:1 cases, the strong enforcement of the data is counter-productive, and amounts to the pointwise forcing of the wrong input! In these cases it is more prudent to enforce the data weakly, so that the more global properties of the solution (like element flux) are preserved on average while no information is enforced in a pointwise manner.

Figure 4 shows the errors $E(t)$ generated for the same parameters as in Figure 3, except that the interface Γ_E is set at $a = 2$ rather than at $a = 5$. Thus, the LM domain here is much smaller. Qualitatively the results are similar to those of Figure 3. A quantitative difference is observed mainly with ME = 4:1. Here the errors are quite larger (but still around or below the 2 per cent level), and the Neumann error increases in time with about the same rate as the Dirichlet and "positive Robin" errors. The increase in the error level is due to the fact that the relative importance of the global information transferred to the LM through the BTO becomes more prominent, since the area of the computational domain decreases while the length of the interface Γ_E remains unchanged. In fact this result, for $a = 2$, is more representative of realistic computations than that of Figure 3 for $a = 5$.

Figure 5 pertains to the case of positive linear reaction, namely $\gamma > 0$. We set $\gamma = 1$. No fundamentally new phenomena are observed here. The results are quite similar to those corresponding to no reaction ($\gamma = 0$), except that the Dirichlet error is slightly larger in this case. With MR = 1:1, the error grows from about 0.2 per cent at $t = 1$ to about almost 0.4 per cent at $t = 4$, while with MR = 4:1, it grows from about 0.8 per cent to above 1.8 per cent, at the same times.

Now we consider negative linear reaction, namely $\gamma < 0$. We note that the negative reaction term has a destabilizing contribution to the heat Equation (5), but as long as $|\gamma|$ is sufficiently small the overall solution is stable. Looking at (60) it is clear that the condition of stability is

$$|\gamma| < \kappa\pi^2\left(\frac{1}{a_{\alpha}^2} + \frac{1}{b^2}\right). \tag{66}$$

We take $\gamma = -0.419$ which satisfies this condition. Figure 6 shows the errors generated in this case. The qualitative picture remains the same, but the errors in this case are smaller than those in the positive reaction case, and in fact even slightly smaller than in the case of no reaction. For example, with a Dirichlet boundary

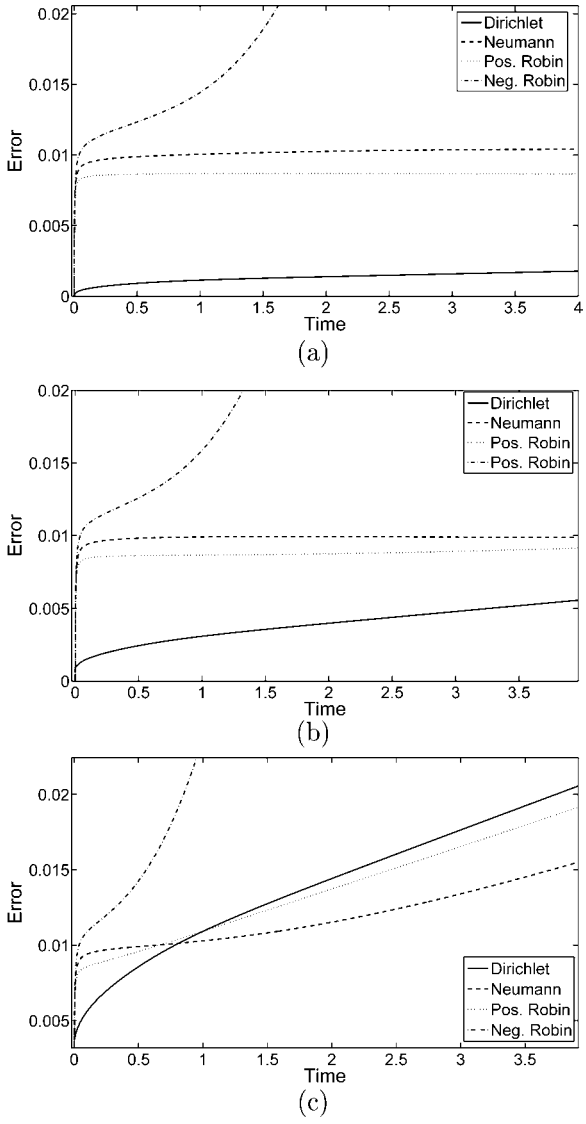

Figure 4.
Error $E(t)$ for $\gamma = 0$, $r = 0$, $a = 2$, with (a) MR $= h_G/h_L = 1$, (b) MR $= 2$, (c) MR $= 4$

condition in the MR = 4:1 case, the error grows from about 0.6 per cent at $t = 1$ to about 1.6 per cent at $t = 4$. This demonstrates the well-known fact that stability and accuracy are entirely different properties; even though we are "closer" to the stability limit in the present case, this does not have any negative effect on the accuracy.

The main conclusions that emanate from these experiments are that the "negative Robin" BTO must be avoided, and that one should prefer the weakly-enforced Neumann and "positive Robin" BTOs over the strongly enforced Dirichlet BTO in actual computations.

As our last accuracy test we consider the nonlinear case of heat emission by radiation ($r \neq 0$) and without reaction ($\gamma = 0$). We set $r = 2$; this value of the radiation

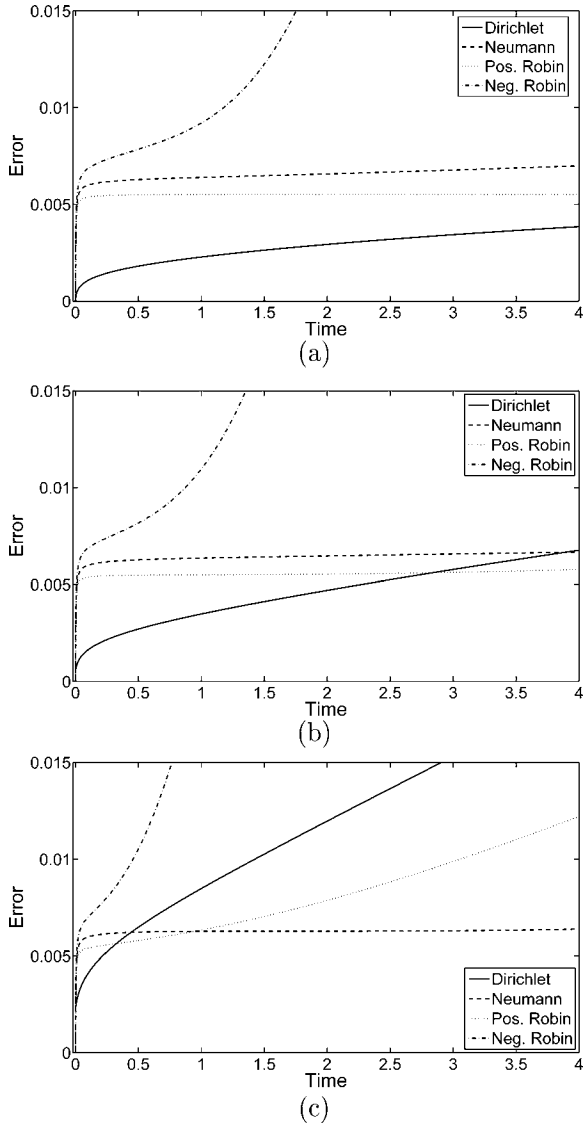

Figure 5.
Error $E(t)$ for $\gamma = 1$, $r = 0$, $a = 5$, with (a) MR $= h_G/h_L = 1$, (b) MR $= 2$, (c) MR $= 4$

coefficient yields a solution which is significantly different than the solution in the linear case, yet convergence is obtained (using Newton iterations within the time step) without any difficulties. Figure 7 shows the errors in this case. It is reassuring to see that the behavior of the error is very similar to that in the linear case, and no new phenomena are observed.

Finally, we consider a problem involving *heterogeneity*. The GM and LM geometry is the same as before, and we take the GM–LM mesh ratio 4:1. The LM material properties are $\kappa = 1$, $\rho c = 1$, $\gamma = 0$ and $r = 0$, except in a single LM element denoted e^* (an "inclusion"), located near the GM–LM interface, whose material properties are

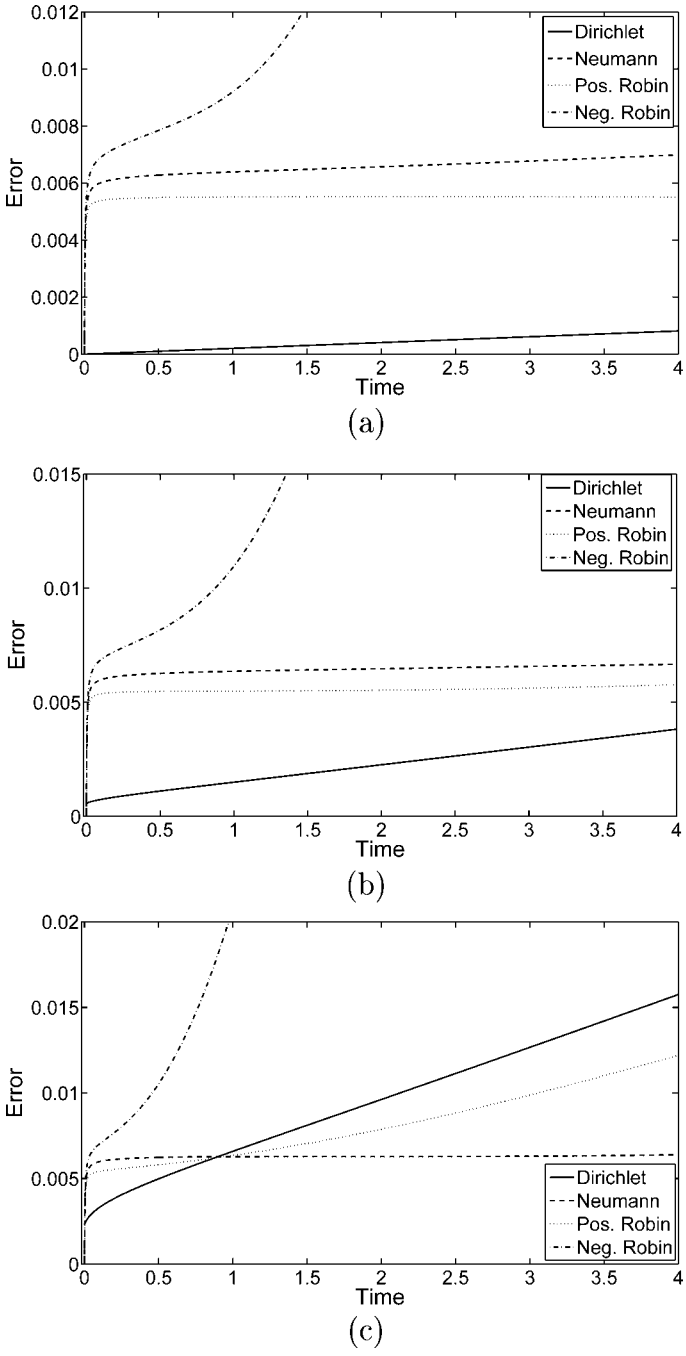

Figure 6.
Error $E(t)$ for $\gamma = -0.419$, $r = 0$, $a = 5$, with (a) MR $= h_G/h_L = 1$, (b) MR $= 2$, (c) MR $= 4$

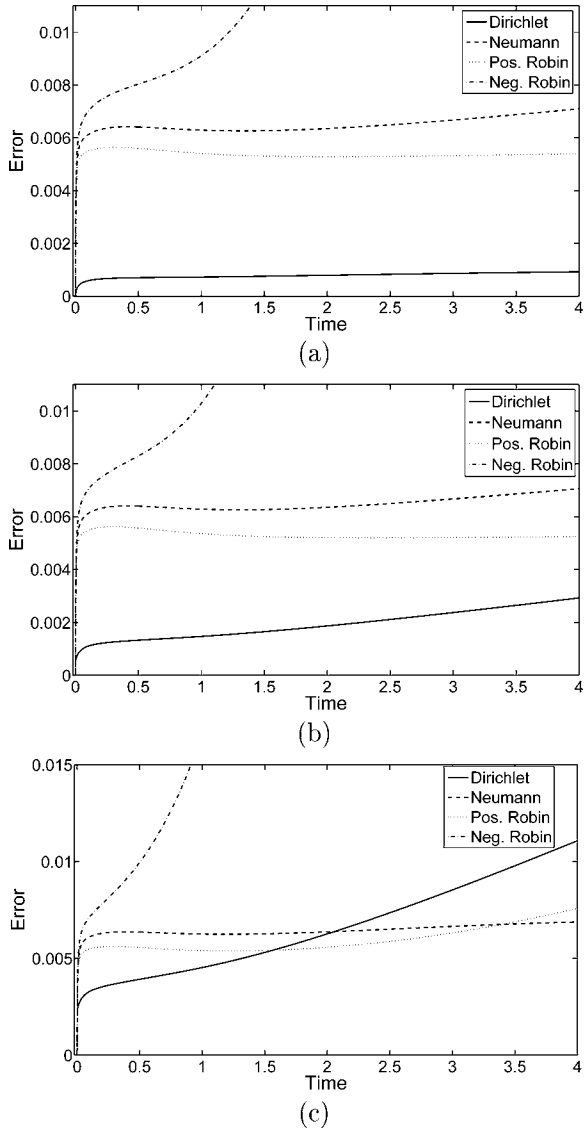

Figure 7.
Error $E(t)$ for $\gamma = 0$, $r = 2$, $a = 5$, with (a) MR $= h_G/h_L = 1$, (b) MR $= 2$, (c) MR $= 4$

significantly different, i.e. $\kappa = 10^4$, $\rho c = 1$, $\gamma = 0$ and $r = 200$. We note that the whole problem is nonlinear due to this single element which emits heat by radiation.

The heterogeneity thus described cannot be resolved by the GM. In order to take it into account nevertheless, we attribute "effective material properties" to the GM element E^* containing the LM element e^*. In E^* the material properties are taken to be $\kappa = 10^4/16$, $\rho c = 1$, $\gamma = 0$ and $r = 200/16$. The factor 1/16 is taken here since the area of e^* is 1/16 than the area of E^*. We use the Neumann operator as the BTO.

Figure 8 shows snapshots at different times of three solutions in the channel; in each plate (a fixed time) the top plot is the reference solution u_{ref}, the middle plot is the GM

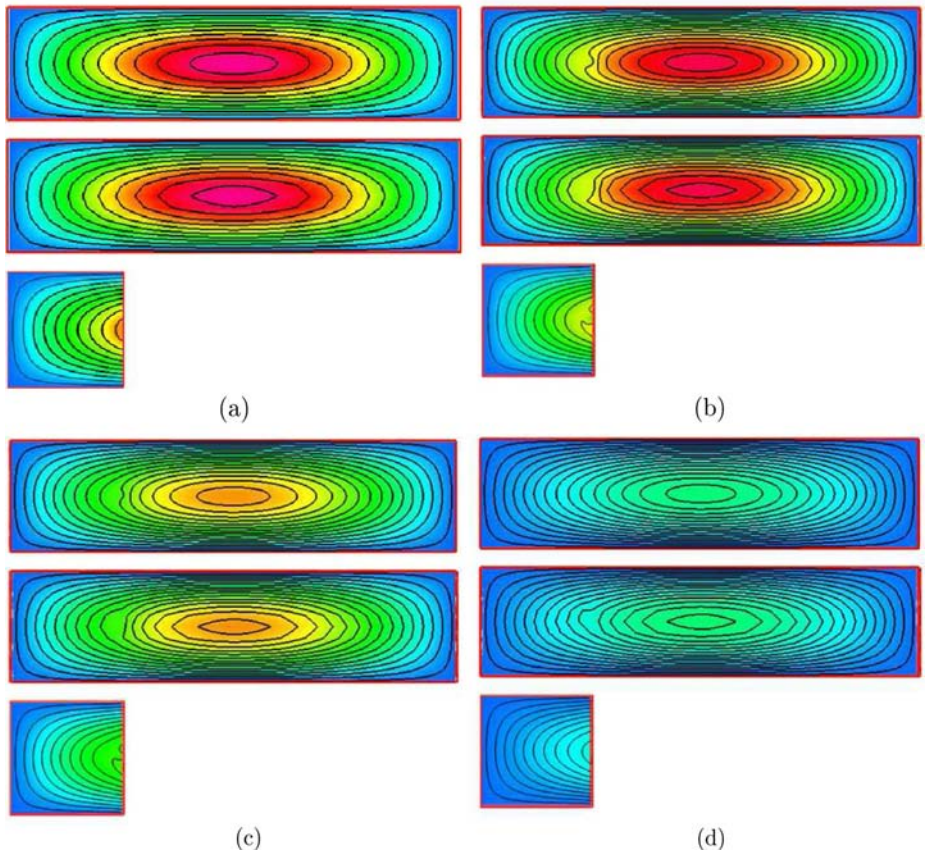

Figure 8.
(a) Snapshots of the temperature distribution in the channel for the heterogeneous problem. (b) In each plate, the top plot is the reference solution u_{ref}, the middle plot is the GM solution u_G, and the bottom plot is the LM solution u_L in the small domain Ω_L. (d) The Neumann operator is used as the BTO. Solutions are shown at times (a) 0, (b) 0.16, (c) 0.78, and (d) 3.12

solution u_G, and the bottom plot is the LM solution u_L in the small domain Ω_L. There is a clear difference in the contour line pattern near the "inclusion" at all times larger than $t = 0$. The LM pattern is much closer to that of the reference solution than the GM pattern. Moreover, at time $t = 3.12$ (Figure 8(d)) diffusive effects cause the local disturbance to completely disappear in the reference solution. Whereas the LM solution also exhibits the same behavior, the GM solution still shows a clear local disturbance which is completely spurious. The implication of this is that the one-way nesting approach works well in this scenario.

6. Concluding remarks

We considered heat flow in a two-dimensional channel with and without radiation and linear reaction, and investigated the performance of various local BTOs in the context of GM–LM interaction, or one-way nesting. We characterized analytically those BTOs which are numerically stable, namely do not give rise to spurious modes. Then we presented some numerical experiments to evaluate the accuracy of four basic BTOs. As mentioned in the introduction, the performance of BTOs has a strong relevance not only to nesting schemes, but also to Domain Decomposition methods in general, since

the BTOs are the basic tool with which information is passed from one part of the global domain to another part of it.

It is interesting to note that the conditions needed to prevent spurious modes that we have found here are significantly more relaxed than those that hold in the case of the hyperbolic *wave equation*; compare the analysis above to that in Mar-Or and Givoli (2006). For wave problems, even the simple Dirichlet and Neumann conditions are associated with spurious modes, and one has to resort to more "exotic" BTOs such as the Sommerfeld operator.

The analysis in this paper was applied to a relatively simple heat-flow model, although our numerical experimentation included the nonlinear (radiation) case. Of course, in Numerical Weather Prediction the situation is much more complicated since the atmospheric system of equations is a nonlinear hyperbolic–parabolic system and involves wave behavior as well as heat flow and other diffusive phenomena. It would be interesting to investigate, at least numerically, various BTOs for more involved benchmarks.

References

Antic, S., Laprise, R., Denis, B. and de Elia, R. (2006), "Testing the downscaling ability of a one-way nested regional climate model in regions of complex topography", *Climate Dynamics*, Vol. 26, pp. 305-325.

Barth, A., Alvera-Azcárate, A., Rixen, M. and Beckers, J.-M. (2005), "Two-way nested model of mesoscale circulation features in the Ligurian Sea", *Progress in Oceanography*, Vol. 66, pp. 171-89.

Bartlett, R.A., Heinkenschloss, M., Ridzal, D. and Waanders, B.V.B. (2006), "Domain decomposition methods for advection dominated linear-quadratic elliptic optimal control problems", *Computer Methods in Applied Mechanics and Engineering*, Vol. 195, pp. 6428-47.

Courant, R. and Hilbert, D. (2004), *Methods of mathematical physics*, Vol. 1, Chapter VI, Wiley, New York, NY.

Davies, H.C. (1976), "A lateral boundary formulation for multi-level prediction models", *Journal of Roy Meteorological Society*, Vol. 102, pp. 405-18.

Drazin, P.G. and Reid, W.H. (2004), *Hydrodynamic Stability*, 2nd ed., Cambridge University Press, Cambridge.

Fish, J. (1992), "The s-version of the finite element method", *Computers and Structures*, Vol. 43, pp. 539-47.

Fox-Rabinovitz, M.S., Cote, J., Dugas, B., Deque, M., McGregor, J. and Gleckler, P. (2005), "The international stretched-grid model intercomparison project (SGMIP), *Proceedings of the 16th Conference on Climate Variability and Change*, American Meteorological Society, available at: http://ams.confex.com/ams/Annual2005/techprogram/paper_83463.htm

Gerardo-Giorda, L., Le Tallec, P. and Nataf, F. (2004), "A Robin-Robin precond ioner for advection-diffusion equations with discontinuous coefficients", Vol. 193, pp. 745-64.

Givoli, D. (1999), Exact representations on artificial interfaces and applications in mechanics", *Applied Mechanics Reviews*, Vol. 52, pp. 333-49.

Haltiner, G.J. and Williams, R.T. (1980), *Numerical Prediction and Dynamic Meteorology*, 2nd ed., Wiley, New York, NY.

Hauret, P. and Le Tallec, P. (2007), "Two-scale Dirichlet-Neumann precond ioners for elastic problems with boundary refinements", *Computer Methods in Applied Mechanics and Engineering*, Vol. 196, pp. 1574-88.

Heinkenschloss, M. and Herty, M. (2007), "A spatial domain decomposition method for parabolic optimal control problems", *Journal of Computational Mathematics*, Vol. 201, pp. 88-111.

Hodur, R.M. (1997), "The naval research laboratory's coupled ocean/atmosphere mesoscale prediction system COAMPS", *Monthly Weather Review*, Vol. 125, pp. 1414-30.

Hughes, J.R. (1995), "Multiscale phenomena – Green's functions, the Dirichlet-to-Neumann formulation, subgrid scale models, bubbles and the origins of stabilized methods", *Computer Methods in Applied Mechanics and Engineering*, Vol. 127, pp. 387-401.

Hughes, T.J.R. (1987), *The Finite Element Method*, Prentice-Hall, Englewood Cliffs, NJ.

Jimenez, P., Parra, R. and Baldasano, J.M. (2007), "Influence of initial and boundary conditions for ozone modeling in very complex terrains: a case study in the northeastern Iberian Peninsula", *Environmental Modelling & Software*, Vol. 22, pp. 1294-1306.

Ju, L.X. and Wang, H.J. (2006), "Modern climate over east Asia simulated by a regional climate model nested in a global gridpoint general circulation model", *Chinese Journal of Geophysics*, Vol. 49, pp. 52-60.

Kalnay, E. (2003), *Atmospheric Modelling, Data Assimilation and Predictability*, Cambridge University Press, Cambridge.

Laprise, R. (2003), "Resolved scales and nonlinear interactions in limited-area models", *Journal of Atmospheric Science*, Vol. 60, pp. 768-79.

Magoules, F., Roux, F.X. and Series, L. (2006a), "Algebraic Dirichlet-to-Neumann mapping for linear elasticity problems with extreme contrasts in the coefficients", *Applied Mathematical Modelling*, Vol. 30, pp. 702-13.

Magoules, F., Roux, F.X. and Series, L. (2006b), "Algebraic approximation of Dirichlet-to-Neumann maps for the equations of linear elasticity", *Computer Methods in Applied Mechanics and Engineering*, Vol. 195, pp. 3742-59.

Mar-Or, A. and Givoli, D. (2006), "The global-regional model interaction problem: analysis of carpenter's scheme and related issues", *International Journal for Multiscale Computational Engineering*, Vol. 4, pp. 617-45.

Mar-Or, A. and Givoli, D. (2009), "High order global-regional model interaction: extension of Carpenter's scheme", *International Journal for Numerical Methods in Engineering*, Vol. 77, pp. 50-74.

Miguez-Macho, G., Stenchikov, G.L. and Robock, A. (2004), "Spectral nudging to eliminate the effects of domain position and geometry in regional climate model simulations", *Journal of Geophysics Research*, Vol. 109, p. D13104.

Phillips, N.A. and Shukla, J. (1973), "On the strategy of combining coarse and fine grid meshes in numerical weather prediction", *Journal of Applied Meteorology*, Vol. 12, pp. 763-70.

Portero, L. and Jorge, J.C. (2005), "Special meshes and domain decomposition methods for evolutionary convection-diffusion-reaction problems", *International Journal of Numerical Methods for Heat and Fluid Flow*, Vol. 47, pp. 1237-43.

Raspo, I., Ouazzani, I J. and Peyret, R. (1996), "A spectral multidomain technique for the computation of the Czochralski melt configuration", *International Journal of Numerical Methods for Heat and Fluid Flow*, Vol. 6, pp. 31-58.

Rosmond, T.E. (1992), "The design and testing of the Navy operational global atmospheric prediction system", *Weather & Forecasting*, Vol. 7, pp. 262-72.

SGMIP: Stretched-Grid Model Intercomparison Project, Earth System Science Interdisciplinary Center, University of Maryland, available at: www.essic.umd.edu/foxrab/sgmip.html

Staniforth, A. (1997), "Regional modelling: a theoretical discussion", *Meteorology and Atmospheric Physics*, Vol. 63, pp. 15-29.

Sundström, A. and Elvius, T. (1979), "Computation problems related to limited-area modeling", in Kasahara, A. (Ed.), *Numerical Methods Used in Atmospheric Models*, World Meteorological Organization, Geneva, Vol. II No. 7, pp. 379-416.

von Storch, H., Langenberg, H. and Feser, F. (2000), "A spectral nudging technique for dynamical downscaling purposes", *Monthly Weather Review*, Vol. 128, pp. 3664-73.

Warner, T.T., Peterson, R.A. and Treadon, R.E. (1997), "A tutorial on lateral conditions as a basic and potentially serious limitation to regional numerical weather prediction", *Bulletin of the American Meteorological Society*, Vol. 78, pp. 2599-617.

Xin, S.H., Duluc, M.C., Lusseyran, F. and Le Quere, P. (2004), "Numerical simulations of natural convection around a line-source", *International Journal of Numerical Methods for Heat and Fluid Flow*, Vol. 14, pp. 830-50.

Yang, J.E. and Yu, D.H. (2006), "Domain decomposition with nonmatching grids for exterior transmission problems via FEM and DTN mapping", *Journal of Computational Mathematics*, Vol. 24, pp. 323-42.

Zienkiewicz, O.C. and Taylor, R.L. (2000), *The Finite Element Method*, 5th ed., Vol. 1, The Basis, Butterworth Heinemann, Oxford.

Corresponding author
Dan Givoli can be contacted at: givolid@aerodyne.technion.ac.il